X-ray and Thermal Studies on the Crystalline Phases of Normal Alkanethiols *n*-$C_nH_{2n+1}SH$ (n=18, 19, 22, 23, 24)

Koji Nozaki[a,*], Masanao Munekane[a,**], Takashi Yamamoto[a] and Yoshihiro Ogawa[b]

[a] *Department of Physics, Faculty of Science, Yamaguchi University, Yamaguchi 753-8512, Japan*

[b] *Department of Science, Faculty of Science, Kumamoto University, Kumamoto 860-8555, Japan*

*Corresponding Author TEL: +81-83-933-5679 FAX: +81-83-933-5273

E-mail nozaki@yamaguchi-u.ac.jp

**Present address: *Engineering Department R&D Department, SII Nanotechnology Inc., Shizuoka 410-1393, Japan*

Abstract

Crystal structures, polymorphism, and phase transitions of five *n*-aklanethiols (*n*-$C_nH_{2n+1}SH$: CnSH), C18SH, C19SH, C22SH, C23SH, and C24HSH have been investigated by means of differential scanning calorimetry and X-ray diffraction. Normal alkanethiols with odd carbon number have only one crystalline form, the E2 form. While, *n*-alkanethiols with even carbon number have two low-temperature crystalline forms, the most stable E1 form and the meta-stable E1' form. When even *n*-alkanethiols are crystallized from the solution (solution growth crystal: SGC), they crystallize into the E1 form. When they are cooled from the melt (melt growth crystal: MGC), on the other hand, the E1' form appears. In all crystalline phases, two *n*-alkanethiol molecules are connected at SH end mutually by hydrogen bond resulting in forming a dimer in both forms. The SH groups and the CH_3 groups are arranged on the respectively different layer surfaces resulting in the bilayer structure in the E1 form. In the E1' form, on the other hand, although the molecules form dimers locally, the SH and methyl groups do not form the one layer surface, respectively, but are arranged disorderly. At temperature just below the melting point, characteristic high-temperature phase, the rotator phase, is observed in even *n*-alkanethiols as well as in *n*-alkane system.

Keywords

alkanethiol, phase transition, crystal structure, X-ray diffraction, polymorph

1. Introduction

Long hydrocarbon chains are constituent of many organic molecules, which are, for example, lipids, fats, oils, and polymers. Therefore, the hydrocarbon plays an important role in the structure formations, such as crystallizations of fats and polymers, formations of lipid membranes, etc. The configurations of the hydrocarbon chains affect the physical properties and the functions of the materials. Therefore, it is very important for the elucidation of biomembrane function or industrial application to understand it. So, many studies, which aimed at a fundamental understanding of the structure formation of the hydrocarbons, have been made using a simple hydrocarbon molecule like *n*-alkane. In the condensation structure of the hydrocarbon chains, it also became clear that similarity is seen at various substance systems [1, 2].

Normal alkanethiol (*n*-$C_nH_{2n+1}SH$) is the hydrocarbon molecule to which the mercapt (-SH) group added at the chain end. It is well known that *n*-alkanethols are the constituent of self-assembled monolaylers (SAM) [3]. Since it was discovered that the *n*-alkanethiol forms SAM on the metal surface such as Au (111) [4, 5], these days, research has come to be briskly done about the packing structure of the molecule, etc [3]. At the present, the application to the pattern formation in the nanotechnology field is also expected. On the other hand, as far as authors know, there is almost no study on the structures of the bulk crystalline phases of *n*-alkanethiol and the phase behavior of it. Thalladi, et al. reported in their paper about the X-ray study using single crystals that *n*-α, ω-alkanedithiol molecules arrange in a similar manner to *n*-alkanes and polyethylene in a crystalline phase [6]. They also revealed that the different molecules have joined together by the intermolecular S…S interaction. In the previous nuclear magnetic resonance (NMR) study on n-alkanethiols [7], it was concluded that the SH chain ends are connected between the different chain ends, and that the intermolecular S…S interaction between SH groups is stronger than the van der Waals interaction between CH_3 groups but weaker than the hydrogen bond between OH groups as well as the covalent bond between CH_2 carbons. Moreover, the differential scanning calorimetry (DSC) study revealed that *n*-alkanethiol crystals show the “rotator (R) phase transition”. In *n*-alkane and some other hydrocarbon molecular crystals, the characteristic high-temperature crystalline phase,

which is so-called the “rotator (R) phase”, appears just below the melting point, and the phase transition between the low-temperature ordered (LO) phase and the R phase (the R phase transition) is usually observed.

In this work, we examine the crystal structures and the phase behaviors of five *n*-aklanethiols with odd and even carbon numbers (18, 19, 22, 23, 24) by using the techniques of differential scanning calorimetry (DSC) and X-ray diffraction. It will be also shown that *n*-alkanethiol demonstrates the different phase transition behavior and polymorph between the odd and even *n*-alkanethiol crystals. The R phase will be observed only for even *n*-alkanethiol crystals and the structure of it is similar to that of *n*-alkane crystals.

Linear hydrocarbon molecules, such as lipids, oils, and polymers, often have the R phases just below their melting points as well as *n*-alkanes [1]. The phase transition between the LO phase and the R phase occurs in *n*-alkanes and these substances [1, 8, 9]. Previously, the structure of the R phase and the phase behavior of them have been studied mainly for *n*-alkane crystals. In the LO phase, *n*-alkane molecules are fully extended taking all-trans conformations and are registrated in layers in which the molecular chain axes are parallel with each other, resulting in three-dimensional crystalline structure. The molecules have the long-range order with respect to both the orientation about their chain axes and their positions. While in the R phase, the molecules still have three-dimensional long-range positional order, but rack the long-range order in the orientation; in spite of their disordered structure, the R phase is indeed crystalline state. The molecules in the R phase make active thermal motion and have high mobility. In particular, the translation along the chain axes and the rotation around the chain axes are excited [10-17]. Recent X-ray investigations have shown the presence of five R phases with different crystal structures. Although they are in solid state, the long-range diffusion of molecules in the R phase was confirmed by means of X-ray diffraction [18] and optical microscopy [19, 20]. These characteristics are expected to relate to various properties of biological membranes constructed by lipids. Hence, in recent years, there has been a growing interest in the R phase and its physical properties.

2. Experimental

Five alkanethiols, *n*-octadecanethiol (*n*-$C_{18}H_{37}SH$: abbreviated C18SH), *n*-nonadecanethiol (*n*-$C_{19}H_{39}SH$: C19SH), *n*-docosanethiol (*n*-$C_{22}H_{45}SH$: C22SH), *n*-tricosanethiol (*n*-$C_{23}H_{47}SH$: C23SH) and *n*-tetracosanethiol (*n*-$C_{24}H_{49}SH$: C24SH), were synthesized by the reaction of alkyl bromide with thiourea in ethanol solution, followed by the decomposition using sodium hydroxide [21]. The purities were 99 % or higher for all alkanethiols used, most of the impurities were homologous molecules with different chain length. Two crystalline powder samples were prepared for each alkanethiol; one was the solution growth crystal (SGC) crystallized from the *p*-xylene solution by slow evaporation of the solvent and the other was the melt growth crystal (MGC) crystallized by slow cooling (<1 °C/min) from the melt.

DSC and X-ray diffraction were made in order to investigate the phase behaviors and the crystal structures. DSC was performed with a standard apparatus (Rigaku, DSC8283) using the powder sample; the typical heating and cooling rate was 1 °C/min. X-ray powder diffraction patterns at room temperature were collected by using a standard diffractometer (Rigaku, RAD-IIA), in which Ni-filtered Cu-Kα radiation was used and each *n*-alkanethiol powder was squeezed into a sample holder. In order to observe the structural change with during heating and cooling, X-ray powder diffraction measurements at various temperatures were also made by Debye-Scherrer method using X-ray diffraction system with imaging plates (Bluker AXS, DIP220); the monochromatic Cu-Kα radiation (40 kV - 250 mA) was used. Each sample powder was put into a glass capillary with diameter of 1.0 mm. Time for exposure was 300 s at each measurement. The temperature of the sample cell was controlled within 0.1°C by a PID controller.

The unit cells of the alkanethiol crystals were determined by means of a single crystal X-ray diffraction method. The single crystals of alkanethiols (SGC) were obtained from *p*-xylene solution. Positions of twenty Bragg peaks were automatically searched using four-circle automatic X-ray diffractometer. The lattice constants were initially determined by means of vector minimization method initially and were refined using the position of the same twenty peaks.

3. Results and Discussion

3.1 DSC

Figs. 1-5 show the DSC thermograms of all *n*-alkanethiol samples investigated here on heating of the SGC (a), those on heating of the MGC (b) and those on cooling from the melt (c), respectively. The phase behavior of *n*-alkanethiol shows an obvious "even-odd effect". In the case of odd *n*-alknethiols, i. e. C19SH (Fig. 2) and C23SH (Fig. 4), both the SGC and the MGC show only one endothermic peak, which is considered to be the melting peak, in the DSC heating curves (Figs. 2(a), 2(b), 4(a) and 4(b)). Moreover, only one exothermic peak that corresponds to crystallization was observed on cooling (Figs. 2(c) and 4(c)). Only one crystalline phase seems to appear for C19SH and C23SH in the observed temperature range.

On the other hand, in the case of even *n*-alkanethiols, i. e. C18SH (Fig. 1), C22SH (Fig. 3) and C24SH (Fig. 5), the phase behaviors are more complicated. First, one endothermic peak was observed for the SGC of every even alkanethiols samples in heating process. This means that the SGC of even alkanethiols melt directly into the liquid state on heating without undergoing a solid-solid phase transition. With regards to MGC, on the other hand, two or more endothermic peaks were observed on heating (Figs. 1(b), 3(b) and 5(b)). The largest endothermic peak at highest temperature is melting peak, and other peaks are considered to correspond to solid-solid phase transitions. When the samples were cooled from the melt, two or more exothermic peaks were observed. It seems that even alkanethiol once crystallizes into a certain solid phase and transforms to a different solid phase; a solid-solid phase transition occurs. Detailed interpretation of these DSC results will be made later with the results of X-ray diffraction.

3.2 Crystal structures

The unit cell of the SGC of C19SH was determined by X-ray diffraction using a single crystal. The SGC of C19SH has a monoclinic structure ($P2_1/a$) with the lattice constants of,

a=0.5607 (0.0009) nm,

b=0.7406 (0.0007) nm,

c=5.3145 (0.0136) nm,

and

β=114.839 (0.127) °,

where parenthetic values are standard deviations. This unit cell is similar to that of the E form of long chain fatty acid crystal [22]. We call this crystalline phase "E2 form" hereafter. A close analysis of the crystal structure was tried after the determination of the unit cell of the E2 form, but a suitable solution could not be obtained due to relatively poor quality of the reflection data except the space of $P2_1/a$. Figs. 6(a) and 6(b) show the X-ray powder diffraction patterns of the MGC and the SGC of C19SH at room temperature, respectively. The positions of the Bragg reflections as well as their d-spacing are listed in Table I. Bragg reflections at $2\theta < 20°$ are 00l reflections from layer stacking. Strong reflections at scattering angles $20° \leq 2\theta \leq 25°$ are $hk0_s$ reflections from side packing of the molecules, where the subscript 's' means the subcell of the C-C-C unit of the hydrocarbon. Bragg reflections on the same raw line near the equator (hk0, hk1, hk2, ···) cannot be resolved because of the short reciprocal axis c*. From the consideration of the unit cell and the observed powder diffraction pattern, it is expected that the crystal structure of alkanethiol is almost similar to that of other hydrocarbon molecular crystals such as n-alkane, n-alcohol, fatty acid, etc.

Figs. 7(a) and 7(b) show a crystal structure of the SGC of C19SH predicted from the X-ray diffraction pattern. Fully extended all-trans hydrocarbon chains are arranged in layers, in which the side packing of the molecules is herringbone type shown in Fig. 7(a). This type of side packing is also observed in orthorhombic polyethylene, n-alkane crystals, fatty acid crystals, etc. Since the c value (5.3145 nm) is near equal to twice the extended molecular length of C19SH, the molecules stack in layers forming dimers by SH-SH interaction (Fig. 7(b)). Although, the relative intensities of the Bragg reflections of the MGC of C19SH (Fig. 6(a)) are different from these of the SGC due to the strong preferred orientation of the MGC sample in the sample cell, the position of the Bragg reflections are consistent with each other. Therefore, in the case of C19SH, it is concluded that the MGC and the SGC have same crystal structure. Hence, E2 form is an exclusive crystalline phase for both the SGC and the MGC of C19SH. This conclusion well explains the results of DSC, too. In the

case of C23SH, which has odd carbons, the results are same as those of C19SH in principle except lattice constants, especially the *c* value. Thus, the odd alkanethiols have only one low temperature crystalline form, the E2 form.

The unit cell of the SGC of C22SH was also determined by means of single crystal X-ray diffraction method. It has monoclinic ($P2_1/a$) unit cell, and the lattice constants are

a=0.5580 (0.0002) nm

b=0.7413 (0.0006) nm

c=6.3918 (0.0016) nm,

and

β=119.139 (0.018) °.

The difference in β angle between odd (C19SH) and even (C22SH) alkanethiols is considered to arise from the different chain end packing.

Figs. 8(a) and 8(b) show x-ray powder diffraction patterns of the MGC and the SGC of C22SH at room temperature, respectively. The positions of the Bragg reflections as well as their *d*-spacing are listed in Table II (SGC) and Table III (MGC).The positions of the 00*l* reflections of them are different from those of the SGC. The interval of the 00*l* positions of the MGC is twice as wide as that of the SGC; this means that the long spacing (stacking period of the layers) of the MGC corresponds to one molecular layer (monolayer). Same results were obtained for other even alkanethiols (C18SH and C24SH). It is also found that the MGC and the SGC of even alkanethiols show different phase behavior on heating, as will be shown in the next section. These results show that, in the case of even alkanetihols, the low-temperature phase of the SGC is different from that of the MGC. Since then, the low-temperature phase of the SGC and that of the MGC of even *n*-alkanethiols are henceforth made to call "E1 form" and "E1' form", respectively. All phase notations using in this paper are summarized as follows: the E1 form is the low-temperature phase of the SGC for even *n*-alkanethiols, the E1' form is that of the MGC for even *n*-alkanethiols, the E2 form is the unique low-temperature phase for odd *n*-alkanethiols.

Long spacing of the layer stacking *L* calculated from the 00*l* positions of *n*-alkanethiol

homologous series is plotted in Fig.9, where L values of C20SH and C21SH were also measured in this work. All L values of the three forms (E1, E1', and E2) individually lie on the three distinct linear lines defined for each form. The long spacing L are represented as L=0.226n+0.629 nm for the E1 form, L=0.119n+0.188 nm for the E1' form, and L=0.228n+0.508 for the E2 form, where n is carbon number. Obvious "even-odd effect" is observed with regards to the long spacing L in n-alkanethiol homologous series. Tilt angles between the molecular chain axes and the normal to the layer surface are estimated from the slopes of above three lines as 27° for the E1 form, 20° for the E1' form, and 26° for the E2 form, respectively, where C-C-C period in the all-trans conformation along the molecular axes is defined to be 0.254 nm.

Crystal structures of n-alkanethiols in the E1, E1', and E2 forms are predicted from above results of X-ray diffraction, and are shown in Figs. 10(a)-(c). For even n-alkanethiols, the side packing of the molecules is herringbone type (Fig. 6) both in the E1 (SGC) and E1' (MGC) forms. The period of the layer stacking in the E1 form is about twice as long as that in the E1' form. Two molecules are connected at SH end mutually by weak hydrogen bond resulting in forming a dimer. The SH groups and the chain-end methyl groups are arranged on the respectively different layer surfaces resulting in the bilayer structure in the E1 form (Fig. 10(a)). In the E1' form, on the other hand, although the molecules form dimers locally, the SH and methyl groups do not form the one layer surface, respectively, but are arranged disorderly. Hence, the layer stacking in the E1' is monolayer which has a period corresponding to the monolayer stacking as an average. The layer stacking is disordered due to the static translational displacement along the chain axes. Therefore, the intensities of the 00l reflections of the E1' form is relatively weak. For odd n-alkanethiols, the crystal structure in the low-temperature E2 form is considered to be similar to that in the E1 form. Side packing is herringbone, and the layer stacking is bilayer. It seems that the difference in the molecular packing between in the E1 and E2 forms arises from the difference in the geometry of the molecules resulting from the even or odd of the carbon numbers, as a result, the lattice constants of two forms are different.

3.3 Phase transitions

Fig. 11(a) shows the temperature dependence of X-ray diffraction pattern of the SGC of the C19SH upon heating. Although the pattern of the initial E2 form at 20°C is not similar to that collected by using a standard diffractometer (Fig. 6), these two patterns are essentially the same, because the positions of Bragg peaks coincide with each other. This seems to be caused by different geometries of the X-ray diffraction method and the different preferred orientation features of the powder samples. When the sample was heated, the diffraction pattern of the E2 form was unchanged below 40°C, and the Bragg peaks completely disappeared at 42°C. It was confirmed that the E2 form directly melts into the liquid phase without any solid-solid phase transitions. X-ray diffraction patterns during cooling from the melt are shown in Fig. 11(b). Crystalline Bragg peaks appeared at 37°C. At 37°C and at 20°C, the 00*l* reflections from the layer stacking in low scattering angle were not observed because of the formation of the heavy preferred orientation, which was caused by the slow crystallization from the melt under a temperature gradient condition in a narrow glass capillary. The relative intensities of the $hk0_s$ reflections ($20 \leq 2\theta \leq 25$) from the side packing are significantly different from those of the E2 form in Figs. 6 and 11(a). This also arose from the significant preferred orientation. Although the relative intensities are different between two patterns in Figs. 11(a) and 11(b) at room temperature, the positions of the Bragg reflections in Figs. 11(a) and 11(b) are well in agreement with each other. Therefore, it is concluded that C19SH crystallizes directly into the E2 form during cooling from the melt. The observation of the X-ray diffraction patterns at various temperatures is consistent with the results of DSC, in which both the SGC and MGC of C19SH show one endothermic peak at 40.1°C on heating and one exothermic peak at 36.6°C on cooling from the liquid phase, where these temperatures are onset points of the peaks. The temperature dependence of the X-ray diffraction pattern of C23SH shows similar result as that of C19SH. Hence, odd *n*-alkanethiols used in this study have only E2 form as a crystalline phase.

Figs. 12(a)-(c) show the temperature dependence of the X-ray diffraction patterns of the SGC of C24SH on heating (a), that on cooling from the melt (b), and that of the MGC on heating, respectively. In the case of the heating process of the SGC (Fig. 12(a)), the Bragg reflections of the

initial E1 form completely disappeared at about 53 °C; the E1 form melted directly into the liquid phase. This result is consistent with the DSC heating thermogram in Fig. 5(a), where only one endothermic peak at 51.9°C was observed. When the C24SH was cooled from the melt (Fig. 12(b)), the crystalline Bragg reflections had been already observable at about 43°C; the crystallization occurred above this temperature. The X-ray diffraction pattern at 43°C is very different from that of the E1 and E1' forms. This pattern is more similar to that of the "rotator phase" which often appears in *n*-alkane and other long chain molecular crystals, usually just below their melting points. Therefore, this high temperature solid phase of C24SH is identified as the rotator phase (R phase). During successive cooling, the X-ray diffraction pattern of the R phase changed into that of the E1' form. That is, the R→E1' phase transition was confirmed by X-ray diffraction. In the DSC curve of C24SH on cooling (Fig. 5(c)), two exothermic peaks at 51.1°C and 40.9°C are found. These peaks can be attributed to the crystallization into the R phase and the solid (R) to solid (E') phase transition, respectively, as compared to the result of the x-ray diffraction in Fig. 12(b). When the C24SH sample crystallized from the melt (MGC), i.e. in the E1' form, was heated again, the X-ray diffraction profile changed into that of the R phase; the E1'→R phase transition was observed. On successive heating, the R phase melted. The two endothermic peaks at 45.1°C and 51.2°C in the DSC heating thermogram (Fig. 5(b)) correspond to the E1'→R transition and the melting, respectively, as compared with the X-ray result in Fig.12(c). It is concluded from above results that the R phase appears for the MGC of C24SH.

Fig. 13 shows the time dependence of X-ray diffraction pattern of C24SH in an isothermal condition at 20°C after cooling from the melt. The pattern soon after the completion of the cooling to 20°C (at t=0 min) is typical one for the E1' from, where the 00l (l=1, 2, 3) reflections were found at about 2θ=3°, 6°, 9° (denoted as 'a' in Fig. 13), respectively. At t=35 min, the 00l reflections of the E1 form (denoted as 'b' in Fig. 13) appeared, and the intensity of them increased with time. This result demonstrates that C24SH undergoes the E1'→E1 transition at room temperature after cooling from the melt. This phase transition seems to proceed faster in the case of shorter alkanethiol. In the case of C18SH, time dependence of the X-ray diffraction pattern at 20° just after cooling from the

melt is shown in Fig. 14. The 00*l* reflections of the E1 form (denoted as 'b' in Fig. 14) had been already found at *t*=0 min as well as the 00*l* reflections of the E1' phase (denoted as 'a' in Fig. 14). In addition, the 00*l* peak intensities of the E1 form showed significant increase with time. When C18SH was cooled from the melt, the sample once crystallized into the R phase and underwent the R→E1' transition during the successive cooling (Fig. 1(c)). Soon after the transition, most of the E1' sample changed into the E1 form in a short time. Hence, it becomes clear that even alkanethiols once crystallize into the R phase and undergo the transition to the meta-stable E1' form during cooling, and that they successively change into more stable E1 form. This change seems to be faster for shorter alkanethiols. Figs. 15 (a) and (b) show DSC heating thermogram of the MGC of C18SH just after cooling from the melt and that after holding the temperature at 20°C for 13 h after the completion of cooling, respectively. In the DSC curve of the heating process immediately after cooling from the melt (Fig. 15 (a), t=0 h), two endothermic peaks near about 27°C and a large one near 30°C were observed. On the other hand, when it was heated after 13 h (Fig. 15 (b)), the endothermic peaks near 27°C were not observed. Figs. 16 (a) and (b) show DSC heating thermograms of the MGC of C18SH measured immediately after cooling from the melt to 20°C and to 25°C, respectively, where the cooling rate was 2 °C/min. As shown in Fig. 1 (c), when C18SH was cooled from the melt, once crystallizing into the R phase, it transformed to the E1' form, but the sample at 25°C was still in the R phase. Therefore, the initial C18SH sample for the DSC measurement of the thermogram in Fig. 16 (b) was in the R phase. A large endothermic peak near 27°C in Fig. 16(b) corresponds to the melting of the R phase clearly. Therefore, the two small endothermic peaks near about 27°C in Fig. 16 (a) are those of the E1'→R transition and the melting of the R phase. Moreover, it is identified that the large endothermic peak near about 30°C in Fig. 16 (a) is that of the melting of the E1 form, which changed from the E1' form near 20°C or during cooling from the melt. All phase transition temperatures of *n*-alkanethiols investigated here are summarized in Table IV, where the transition temperatures were determined from the DSC heating curves.

Figs. 17 (a)-(d) show DSC heating curves of C18SH immediately after cooling from the

melt to 20°C with various cooling rates. With an increase in cooling rate, the fraction of the E1 form at room temperature increased. It was confirmed that some of the E1' crystallites transform to the most stable E1 form during cooling. In this case, only the crystallites in which the nucleus of the E1 form happens to generate can give rise to the E1'→E1 transition. In the case of the solid-solid phase transition, the nucleation of the daughter phase is considered to occur in the region of the defect, the accumulation of the strain, and so on, in the parent phase [23]. The primary nucleation barrier is considered to be low in such regions resulting in the high nucleation rate; the nucleation occurs heterogeneously. Probably, in present case, the nucleation is closely related to the accumulation of the strain in the E1' form. When the cooling rate is high, the accumulation of the strain in the E1' becomes significant. Therefore, the nucleation rate is higher with an increase in cooling rate. As a result, the fraction of the E1 form of C18SH at room temperature after cooling form the melt increases. About this result, the consideration of beyond this is impossible.

Relative free energy diagram of the alkanethiol with even carbon number is predicted and shown in Fig. 18. When the SGC in the most stable E1 form is heated, it melts directly into the liquid phase at T_m^{E1} (line 'a' in Fig. 18). If it is cooled from the melt, alkanethiol once crystallizes into the R phase and transforms to the E1' form (line 'b') successively. When the MGC in the E1' form is heated again it changes into the R phase at $T_{E1'\rightarrow R}$ and melts at T_m^R (line 'c'). The meta-stable E1' form prepared by cooling from the melt transforms to the most stable E1 form continuously when the temperature is hold at room temperature (line 'd'). The rate of the transformation tends to become remarkably quick for small carbon number.

Fig. 19 shows the speculated structural change in the E1' → E1 phase transition. The dimer molecules in the E1' form makes translation along the chain axes, and the SH groups of the molecules may be arranged with the same side of the layer plane. Thus, the reordering of the molecular arrangement in the E1'→E1 transition proceeds. Although it may also explain this reordering phenomenon that each molecule makes rotation around its center within the E1' form crystal and SH groups are arranged in same layers, if it takes into consideration that the E1'→E1 transition occurs at low temperature, the rearrangement model by advancing side-by-side movement

along the molecular axes is appropriate to this structural change. It is thought that the chain sliding diffusion motion [24, 25] along the molecular axes takes place during the ordering process in the crystallization of linear polymer, and this result is an example of the formation by the reordering which just takes place by the molecular diffusion. Hence, in relevance with the crystallization of linear polymer, it is an interesting result.

4. Conclusions

We have studied the crystal structures, the polymorphism, and the phase transitions of *n*-alkanethiols, C18SH, C19SH, C22SH, C23SH, and C24SH, by means of DSC and X-ray diffraction. The major results are summarized as follows.

It is confirmed from the results of X-ray diffraction experiments and DSC measurements that *n*-alkanethiols with odd carbon number used in this work have only one crystalline phase, the E2 form. In the case of *n*-alkanethiols with even carbon number, on the other hand, two low-temperature phases, the E1 and E1' forms appears. Polymorphism is observed for even *n*-alkanethiol crystals. When even *n*-alkanethiol is crystallized from the solution, i. e. in the case of the SGC sample, it crystallized into the most stable E1 form. When it is cooled from the melt, i. e. in the case of the MGC sample, the meta-stable E1' form once appears at room temperature and changes into the most stable E1 form continuously. In all crystalline phases of *n*-alkanethiol, two molecules are connected at SH end mutually by hydrogen bond resulting in forming a dimer in both forms. The SH groups and the CH_3 groups are arranged on the respectively different layer surfaces resulting in the bilayer structure in the E1 form. In the E1' form, on the other hand, although the molecules form dimers locally, the SH and methyl groups do not form the one layer surface, respectively, but are arranged disorderly. The structural change in the E1' → E1 phase transition is characterized by the ordering of the layer structure by the translational diffusive motion along the chain axes of the molecules. The characteristic high-temperature phase, the R phase, which is similar to the rotator phase observed for *n*-alkane crystals, appears for even *n*-alkanethiols, and the E1' → R is observed on heating by means of X-ray diffraction. While, when the E1 form is heated, it directly melts into the liquid phase.

Acknowledgments

This work was supported by a Grant-in-Aid for Scientific Research (No. 14540378) from the Ministry of Education, Culture, Sports, Science and Technology.

References

1. B. M. CRAVEN, Y. LANGE, G. G. SHIPLEY, and J. STEINER, in "Handbook of Lipid Research, Vol. 4", edited by D. M. Small (Plenum, New York, 1986).

2. E. B. SIROTA, *Langmuir* **13** (1997) 3849.

3. A. ULMAN, in "An Introduction to Ultrathin Organic Films From Langmuir-Blodgett to Self-Assembly", (Academic Press, San Diego, 1991).

4. M. D. PORTER, T. B. BRIGHT, D. L. ALLARA, and C. E. D. CHIDSEY, *J. Am. Chem. Soc.* **109** (1987) 3559.

5. C. D. BAIN, E. B. TROUGHTON, Y. –T. TAO, J. EVALL, G. M. WHITESIDES, and R. G. NUZZO, *J. Am. Chem. Soc.* **111** (1989) 321.

6. V. R. THALLADI, R. BOESE, H. –C. WEISS, *J. Am. Chem. Soc.* **122** (2000) 1186.

7. K. KUWABARA, F. HORII, Y. OGAWA, *J. Mol. Struct.* **79** (2002), 79.

8. M. G. BROADHURST, *J. Res. Natl. Bur. Stand. Sect.* **A66** (1962) 241.

9. A. MÜLLER, *Proc. R. Soc. London Ser.* **A138** (1932) 514.

10. J. DOUCET, I. DENICOLO and A. GRAIEVICH, *J. Chem. Phys.* **75** (1981) 1523.

11. J. DOUCET, I. DENICOLO, A. GRAIEVICH and A. COLLET, *J. Chem. Phys.* **75** (1981) 5125.

12. I. DENICOLO, J. DOUCET and A. F. GRAIEVICH, *J. Chem. Phys.* **78** (1983) 1465.

13. J. DOUCET, I. DENICOLO, A. F. GRAIEVICH and C. GERMAIN, *J. Chem. Phys.* **80** (1984) 1647.

14. G. UNGAR, *J. Phys. Chem.* **87** (1983) 689.

15. G. UNGAR and N. MAŬIĆ, *J. Phys. Chem.* **89** (1985) 1036.

16. E. B. SIROTA, H. E. King Jr., D. M. SINGER and H. H. Shao, *J. Chem. Phys.* **98** (1993) 5809.

17. E. B. SIROTA and D. M. SINGER, *J. Chem. Phys.* **101** (1996) 10873.

18. T. YAMAMOTO and K. NOZAKI, *Polymer* **35** (1994) 3340.

19. T. YAMAMOTO and K. NOZAKI, *Polymer* **36** (1995) 2505.

20. T. YAMAMOTO, T. AOKI, S. MIYAJI and K. NOZAKI, *Polymer* **38** (1997) 2643.

21. G. G. URQUHART, J. W. GATES and R. CONNOR, *Org. Synth. III* (1955) 363.

22. F. KANEKO, M. KOBAYASHI, Y. KITAGAWA, Y. MATSUURA and Y. KATSUBE, *Acta Crystallogr.*, **C46** (1990) 1490.

23. K. NOZAKI and M. HIKOSAKA, *J. Mater. Sci.*, **35** (2000) 1239.

24. M. HIKOSAKA, *Polymer*, **28** (1987) 1257.

25. M. HIKOSAKA, *Polymer*, **31** (1990) 458.

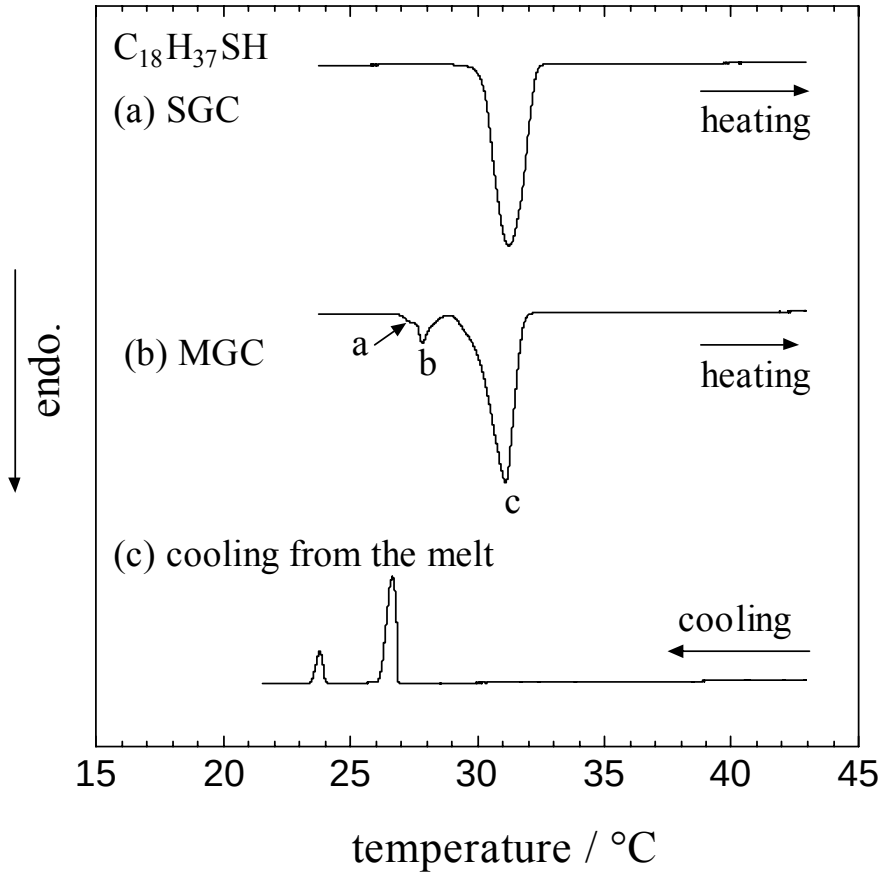

Figure1 DSC heating thermograms of C18SH samples, (a) SGC and (b) MGC, and (c) DSC thermogram during cooling from the melt.

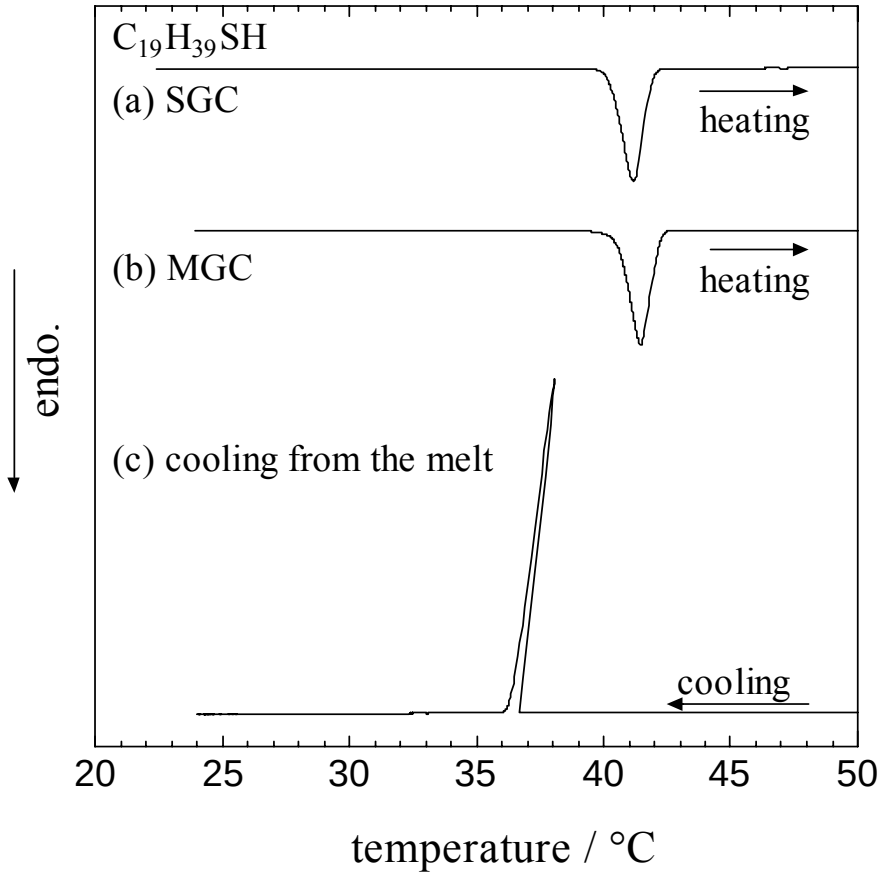

Figure 2 DSC heating thermograms of C19SH samples, (a) SGC and (b) MGC, and (c) DSC thermogram during cooling from the melt.

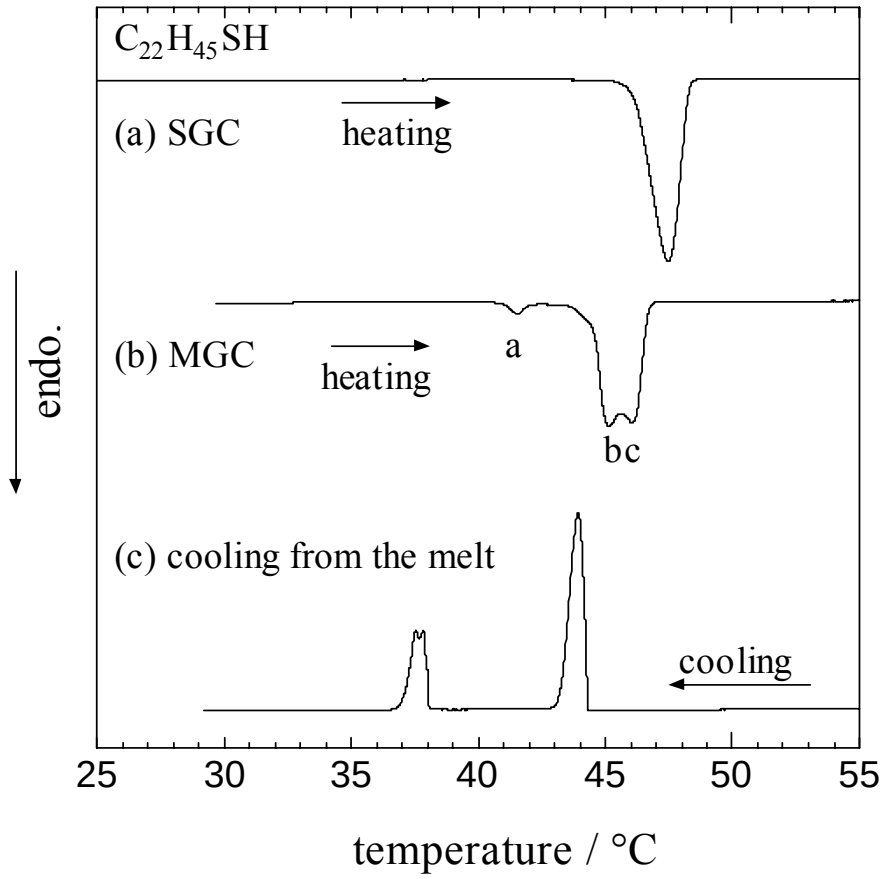

Figure 3 DSC heating thermograms of C22SH samples, (a) SGC and (b) MGC, and (c) DSC thermogram during cooling from the melt.

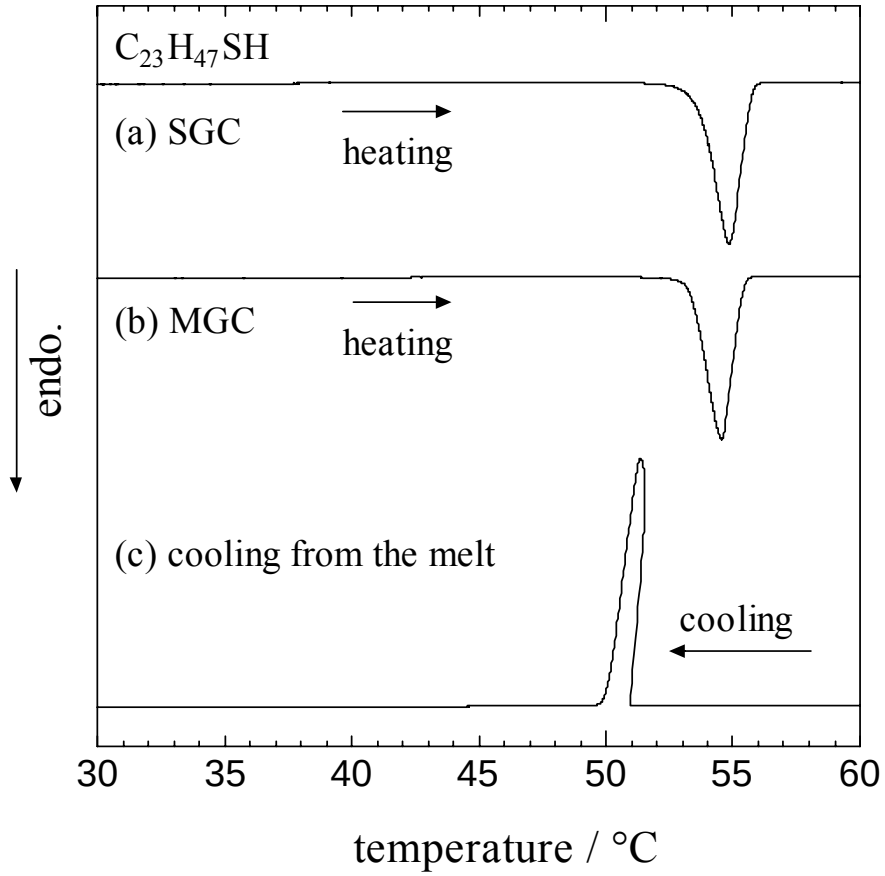

Figure 4 DSC heating thermograms of C23SH samples, (a) SGC and (b) MGC, and (c) DSC thermogram during cooling from the melt.

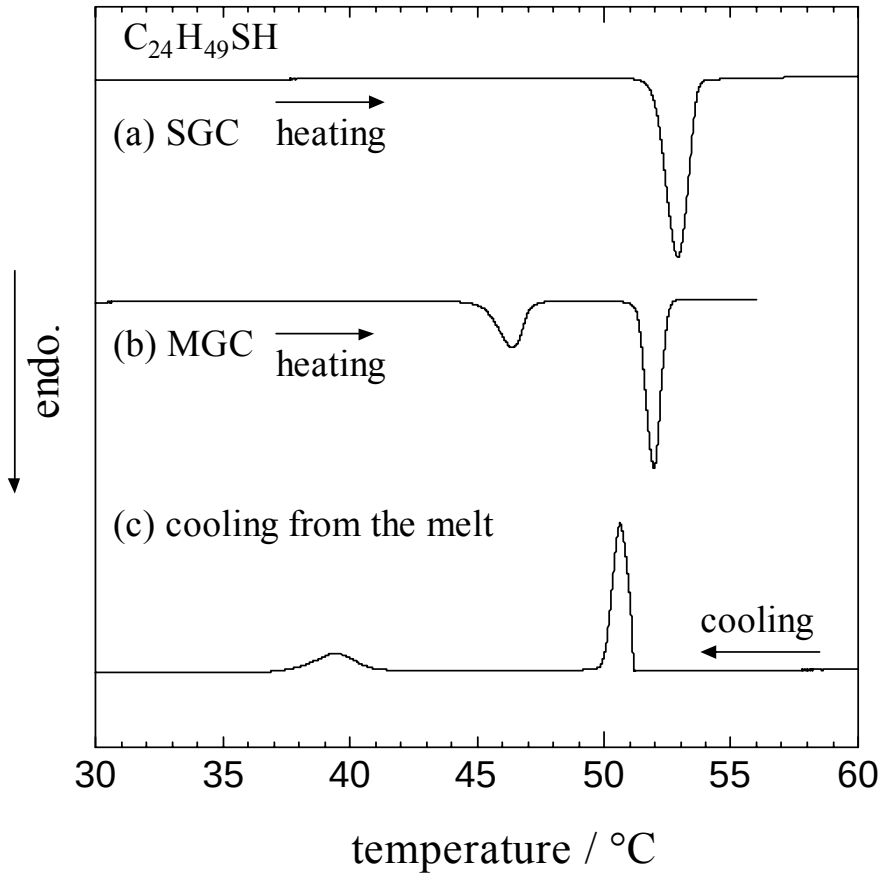

Figure 5 DSC heating thermograms of C24SH samples, (a) SGC and (b) MGC, and (c) DSC thermogram during cooling from the melt.

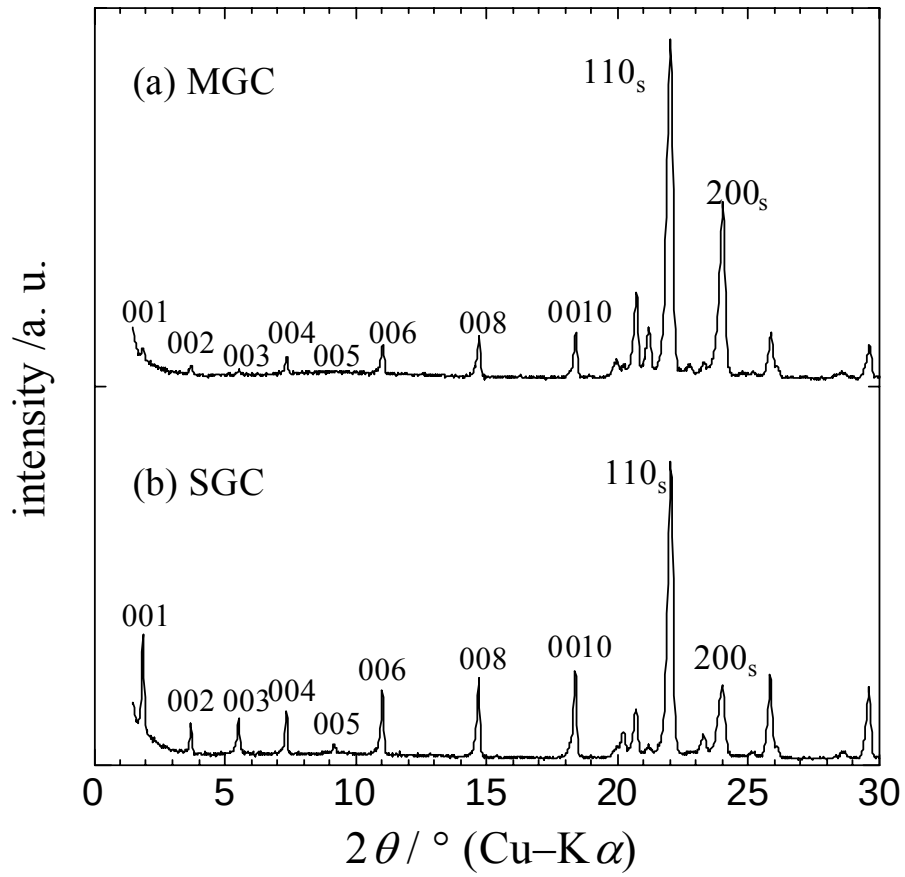

Figure 6 X-ray diffraction patterns of C19SH powder samples, (a) MGC and (b) SGC, at room temperature. The Bragg peaks at scattering angles $2\theta < 20°$ are 00*l* reflections from the layer stacking, and the two strong peaks at angles $20° < 2\theta < 25°$ are $hk0_S$ reflections from the side packing, where subscript 's' means the subcell of the C-C-C unit.

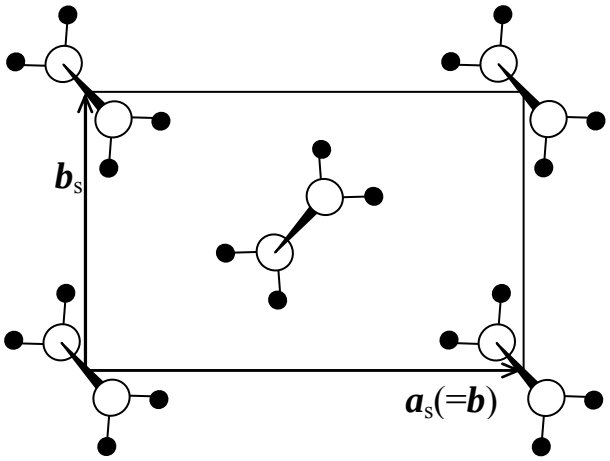

(a)

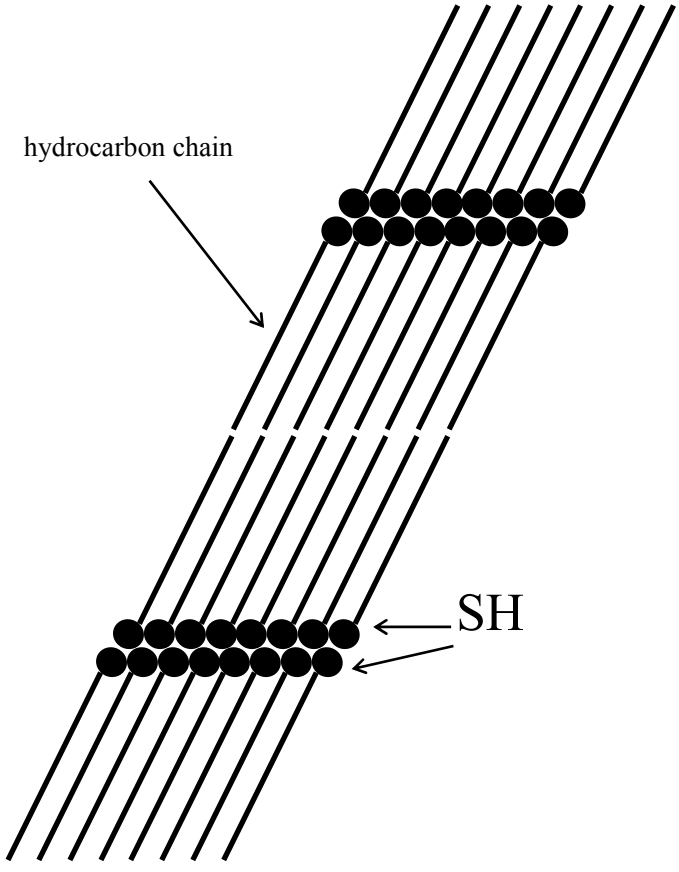

(b)

Figure 7 Possible crystal structure predicted from X-ray powder diffraction pattern of the SGC of C19SH. Fully extended all-trans hydrocarbon chains are arranged in layers, in which the side packing of the molecules is herringbone type (a). The molecules stack in layers forming dimers by SH-SH interaction (b).

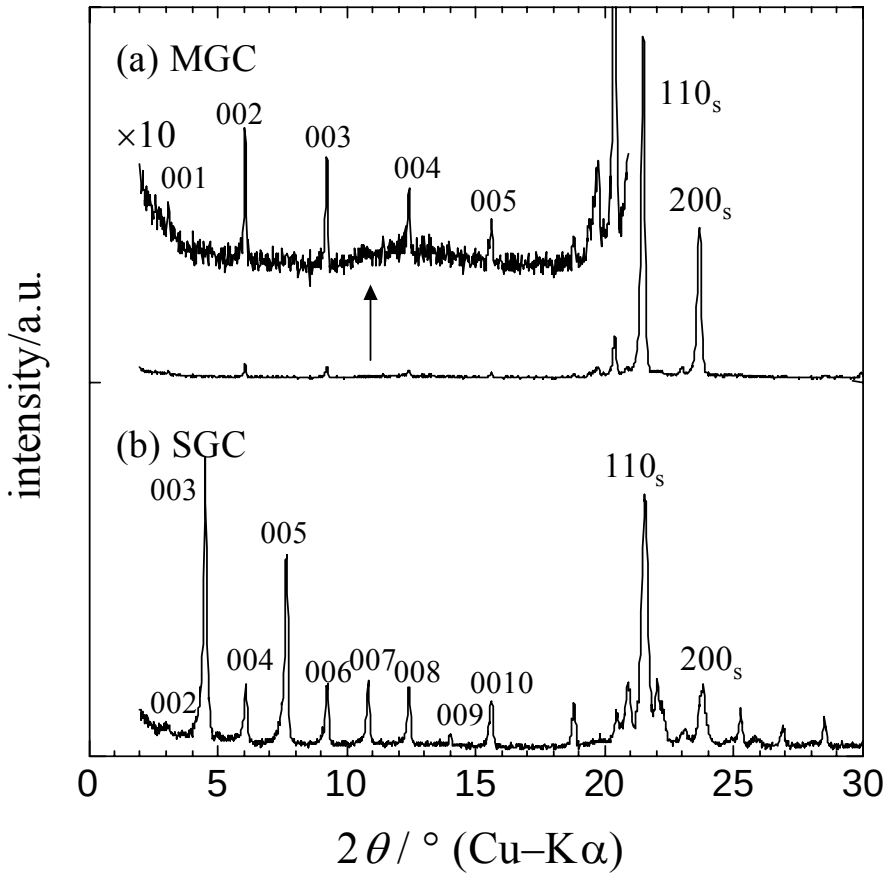

Figure 8 X-ray diffraction pattern of C22SH powder samples, (a) MGC and (b) SGC, at room temperature. The interval of the 00*l* Bragg reflections of the MGC (a) is twice as wide as that of the SGC (b).

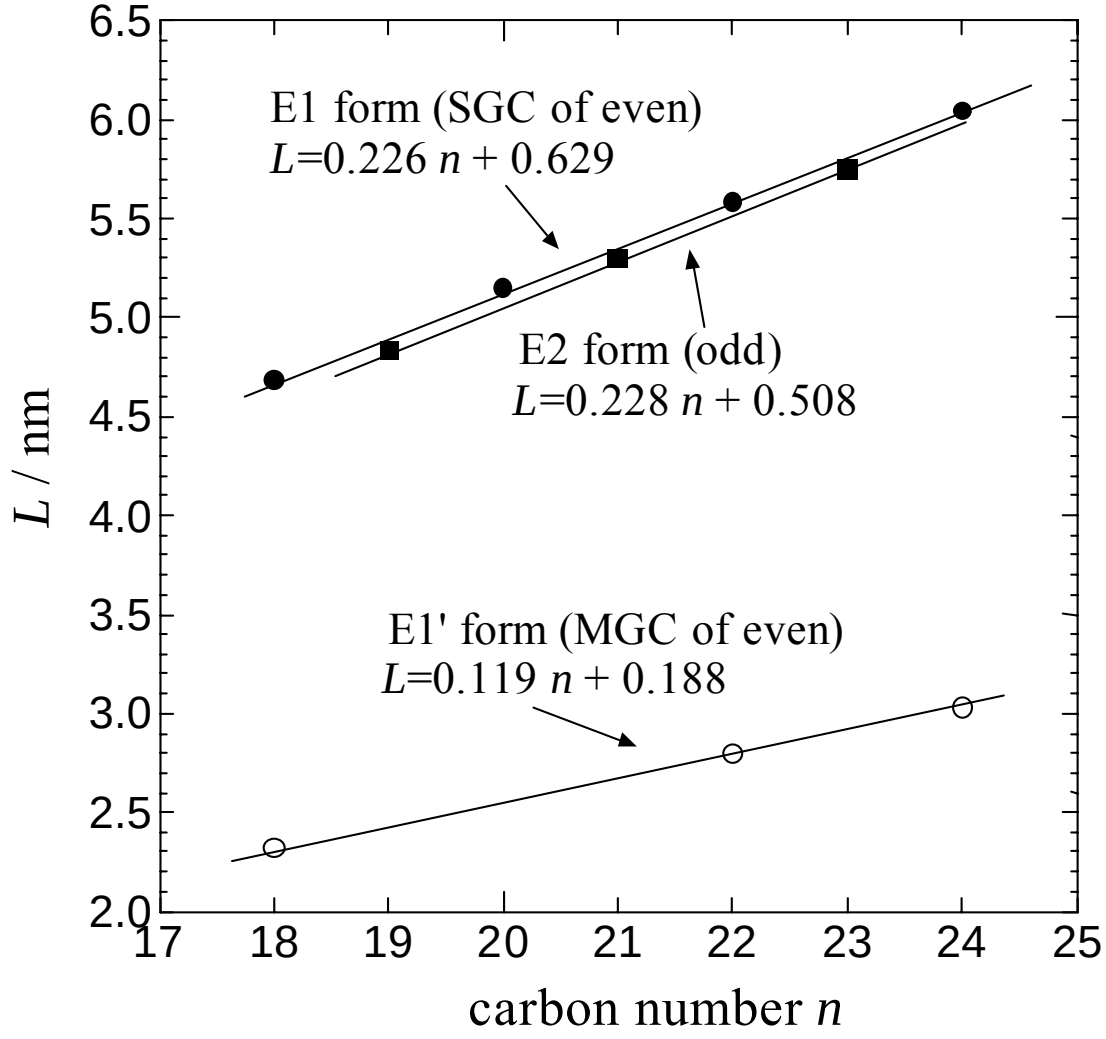

Figure 9 Long spacing of layer staking, *L*, vs. carbon number, *n*, of *n*-alkanethiol homologous series. All L values of the three crystalline forms (E1, E1', and E2) individually lie on the three distinct linear lines defined for each form, respectively. The long spacing *L* are represented as L=0.226n+0.629 nm for the E1 form, L=0.119n+0.188 nm for the E1' form, and L=0.228n+0.508 for the E2 form. L values od C20SH and C21SH were also measured in this work.

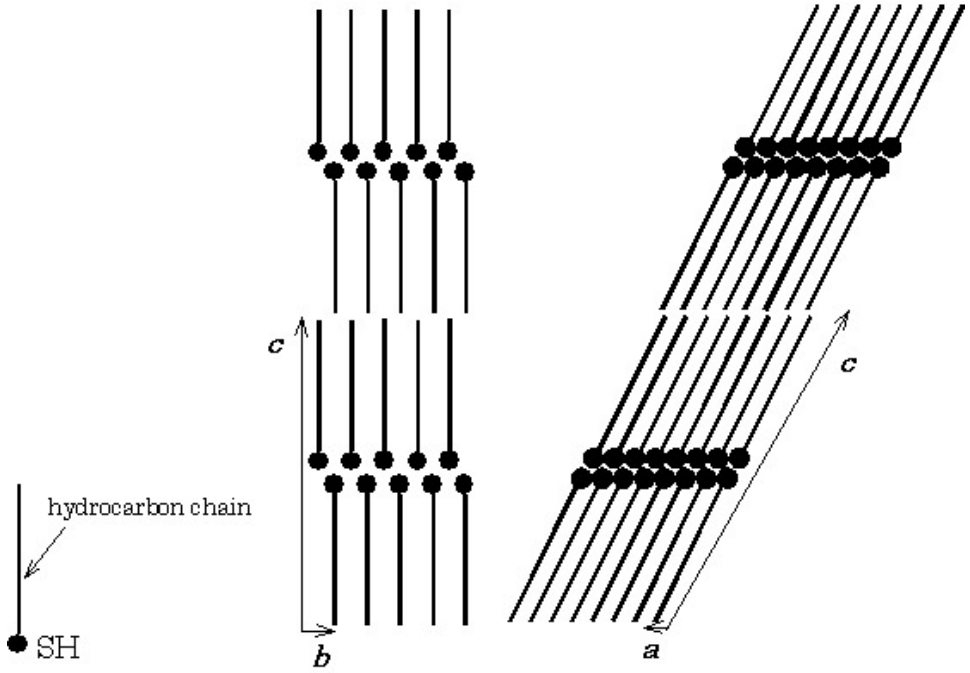

(a)

Figure 10 Crystal structures of *n*-alkanethiols in the (a) E1, (b) E1', and (c) E2 forms predicted from the results of X-ray diffraction. Unitcells in the three forms are monoclinic, but the lattice constants are different. The side packing of the molecules is herringbone type in all forms. Two molecules are connected at SH end mutually by weak hydrogen bond resulting in forming a dimer. The SH groups and the chain-end methyl groups are arranged on the respectively different layer surfaces resulting in the bilayer structure in the E1 form (a) and the E2 form (c). In the E1' form (b), on the other hand, although the molecules form dimers locally, the SH and methyl groups do not form the one layer surface, respectively, but are arranged disorderly. Hence, the layer stacking in the E1' is monolayer which has a period corresponding to the one molecular layer as an average.

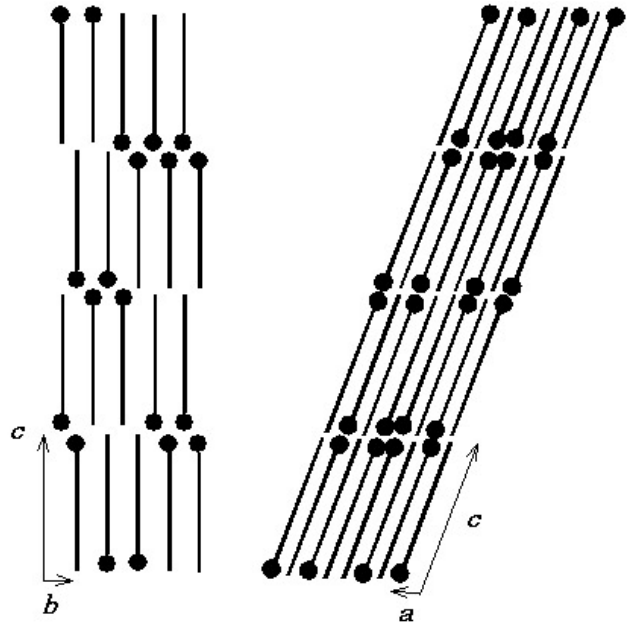

(b)

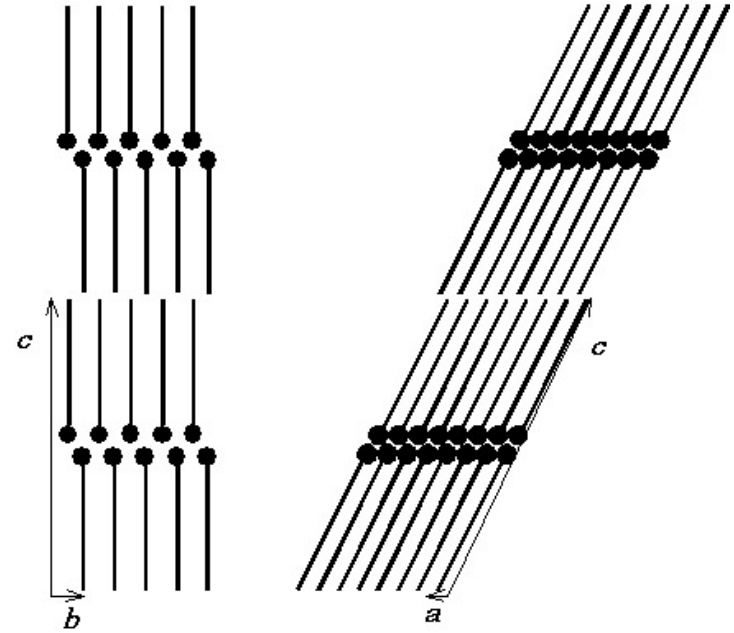

(c)

（***Figure 10*** continued）

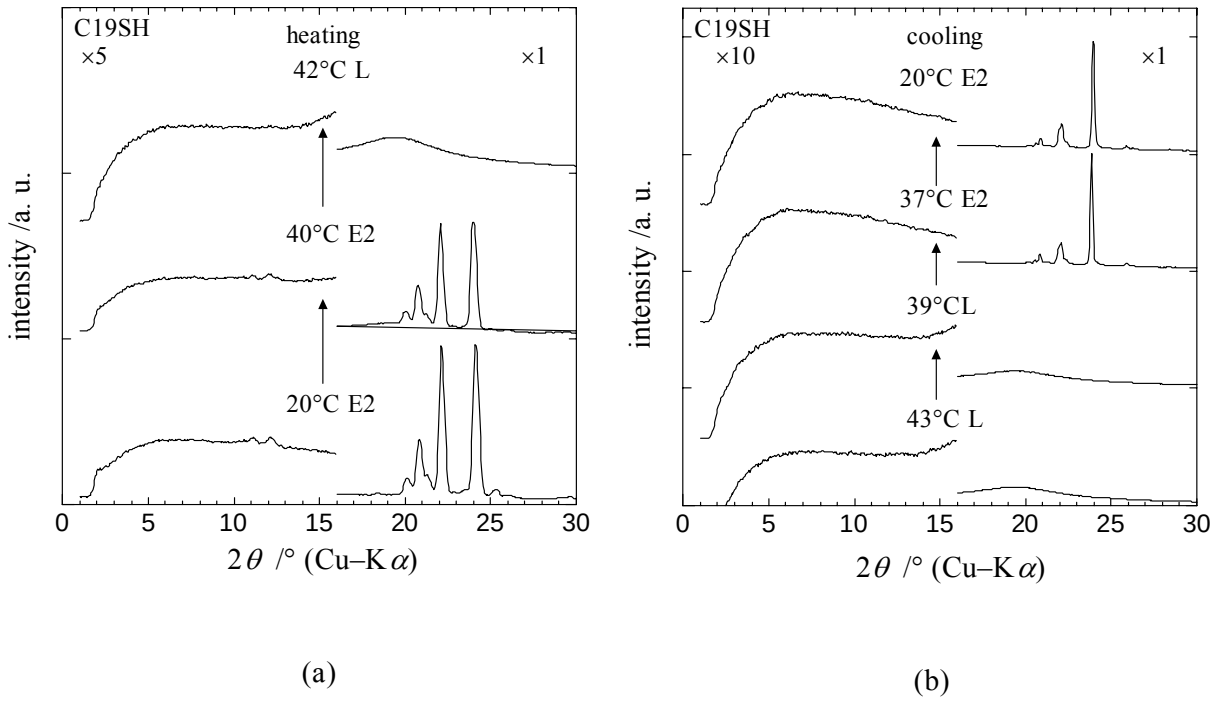

Figure 11 Temperature dependences of X-ray powder diffraction pattern of C19SH, (a) on heating of the E2 form (SGC) and (b) during cooling from the melt. The pattern of the initial E2 form (SGC) at 20°C (a) and that final E2 form (MGC) at 20°C (b) are significant different due to the different preferred orientation features, but the positions of all Bragg peaks in two patterns are same.

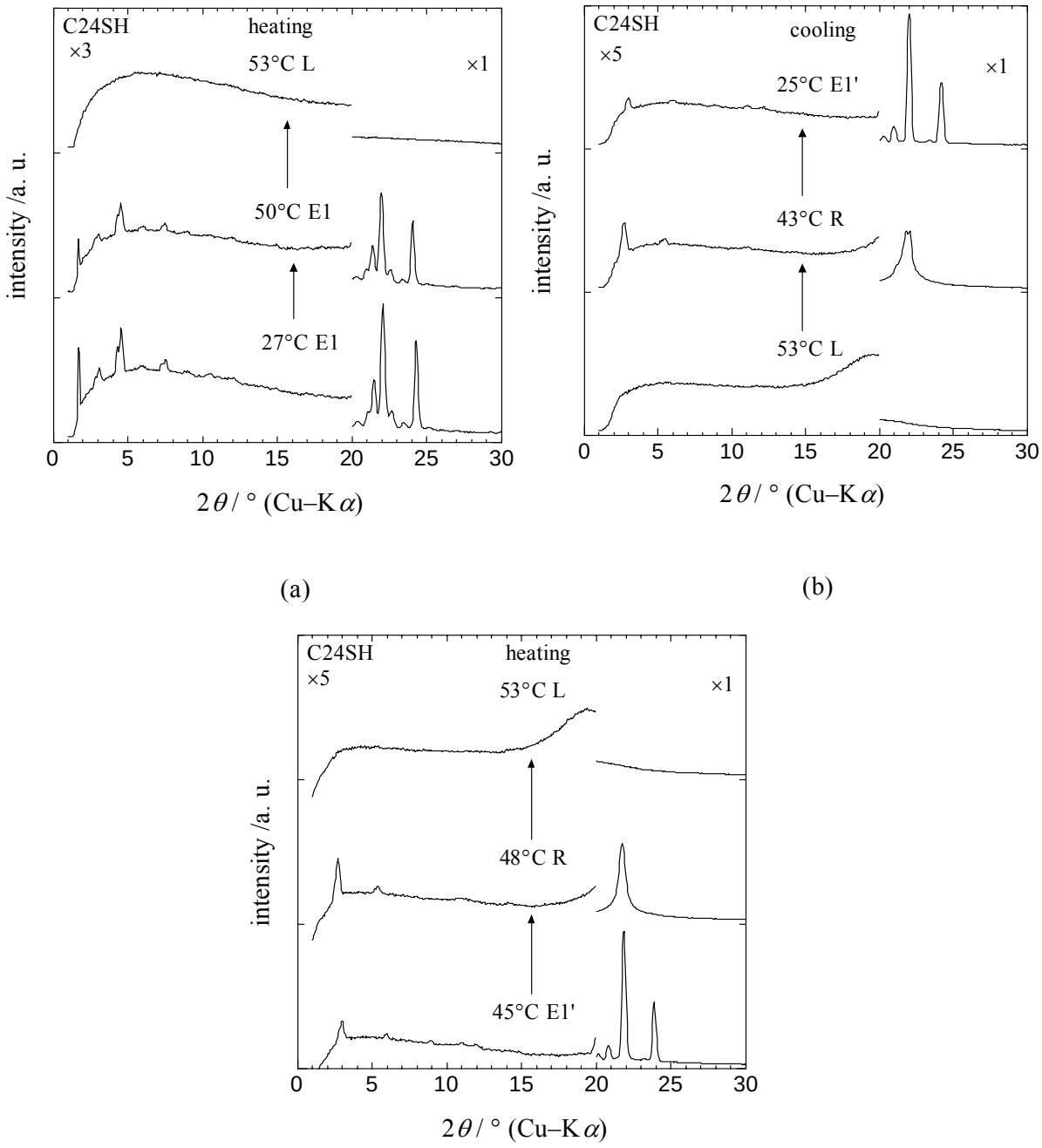

Figure 12 Temperature dependences of the X-ray diffraction pattern of (a) the SGC of C24SH on heating, (b) that during cooling from the melt, and (c) that of the MGC on heating, respectively.

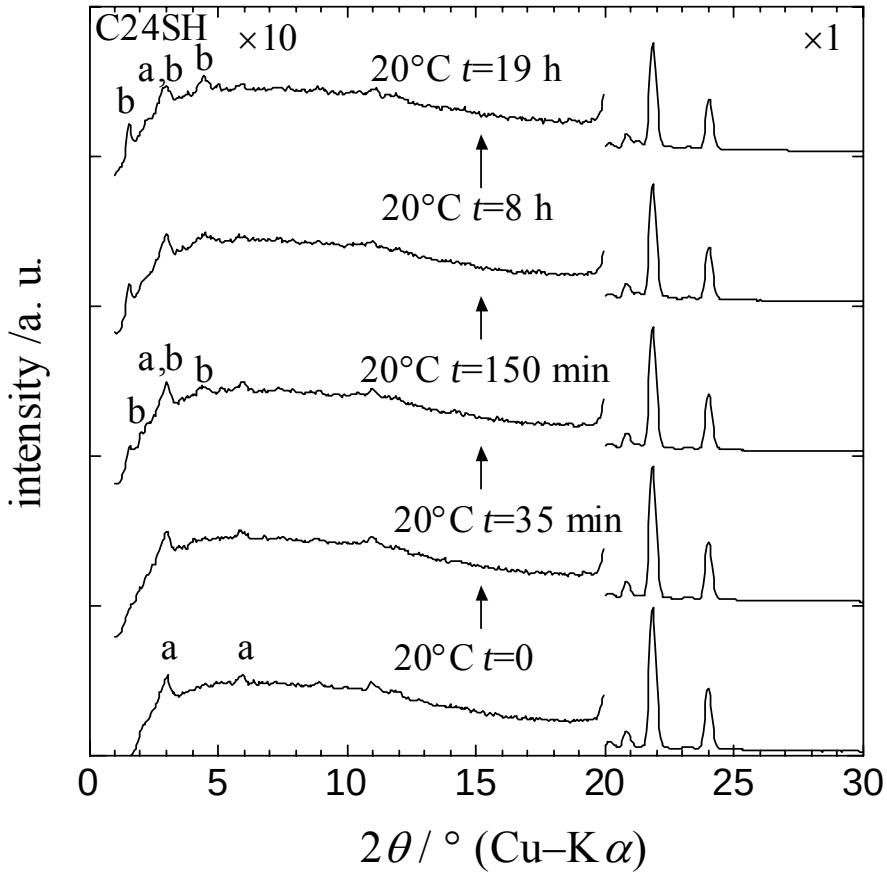

Figure 13 Time dependence of X-ray diffraction pattern of C24SH in an isothermal condition at 20°C after cooling from the melt. A series of the 00*l* reflections denoted as 'a' correspond to the long period reflections from the layer stacking of the E1' form. On the other hand, the 00*l* reflections seen after *t* =35 min (denoted as 'b') are the long period reflections of the E1 form.

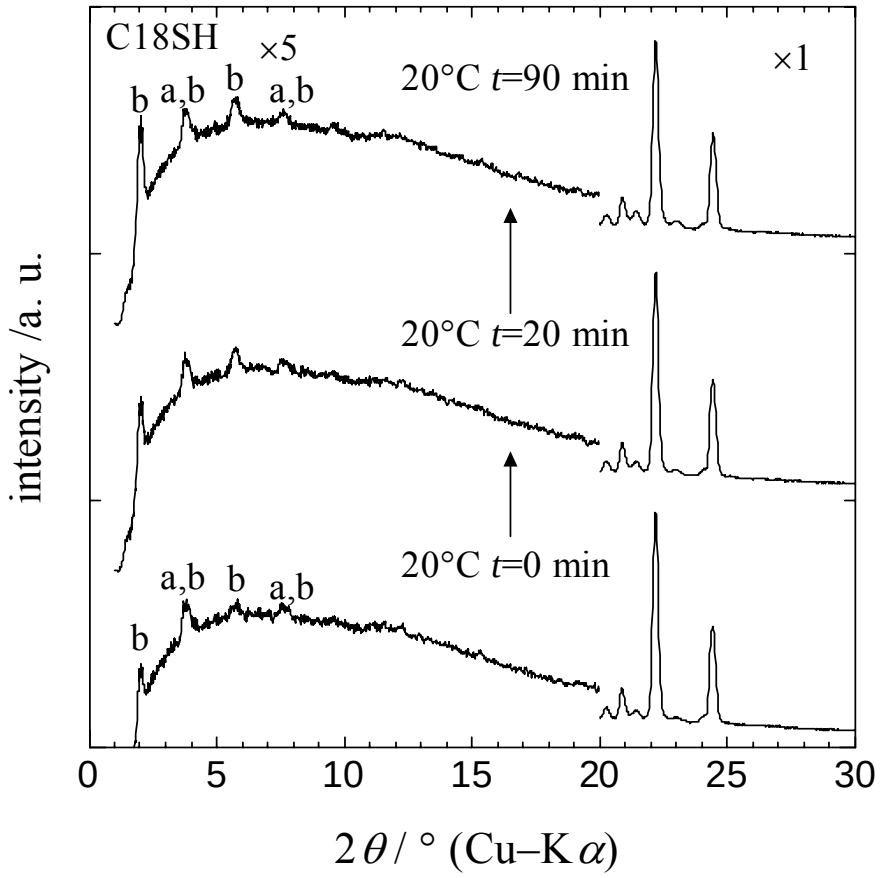

Figure 14 Time dependence of X-ray diffraction pattern of C18SH in an isothermal condition at 20°C after cooling from the melt. The 00*l* reflections denoted as 'a' and those denoted as 'b' correspond to the long period reflections from the layer stacking of the E1' form and those of the E1 form, respectively.

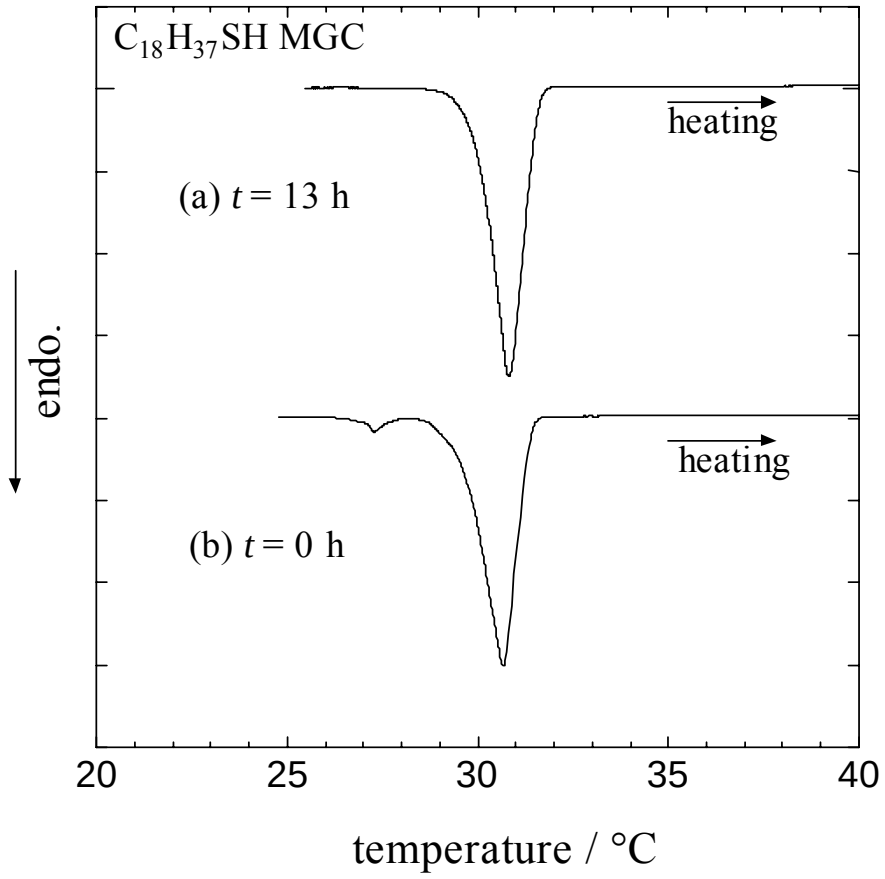

Figure 15 DSC heating thermogram of the MGC of C18SH, (a) just after cooling from the melt, and (b) that after holding the temperature at 20°C for 13 h after the completion of cooling from the melt.

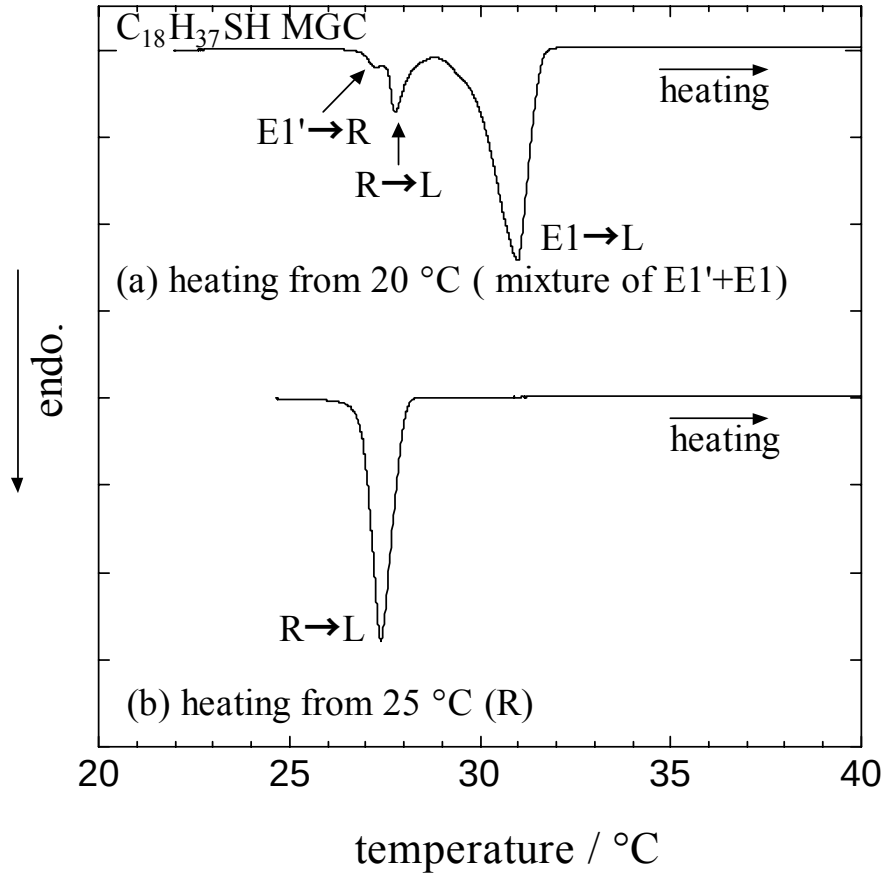

Figure 16 DSC heating thermograms of the MGC of C18SH measured immediately after cooling from the melt, (a) to 20°C, and (b) to 25°C, respectively. The cooling rates during both measurements were 2 °C/min.

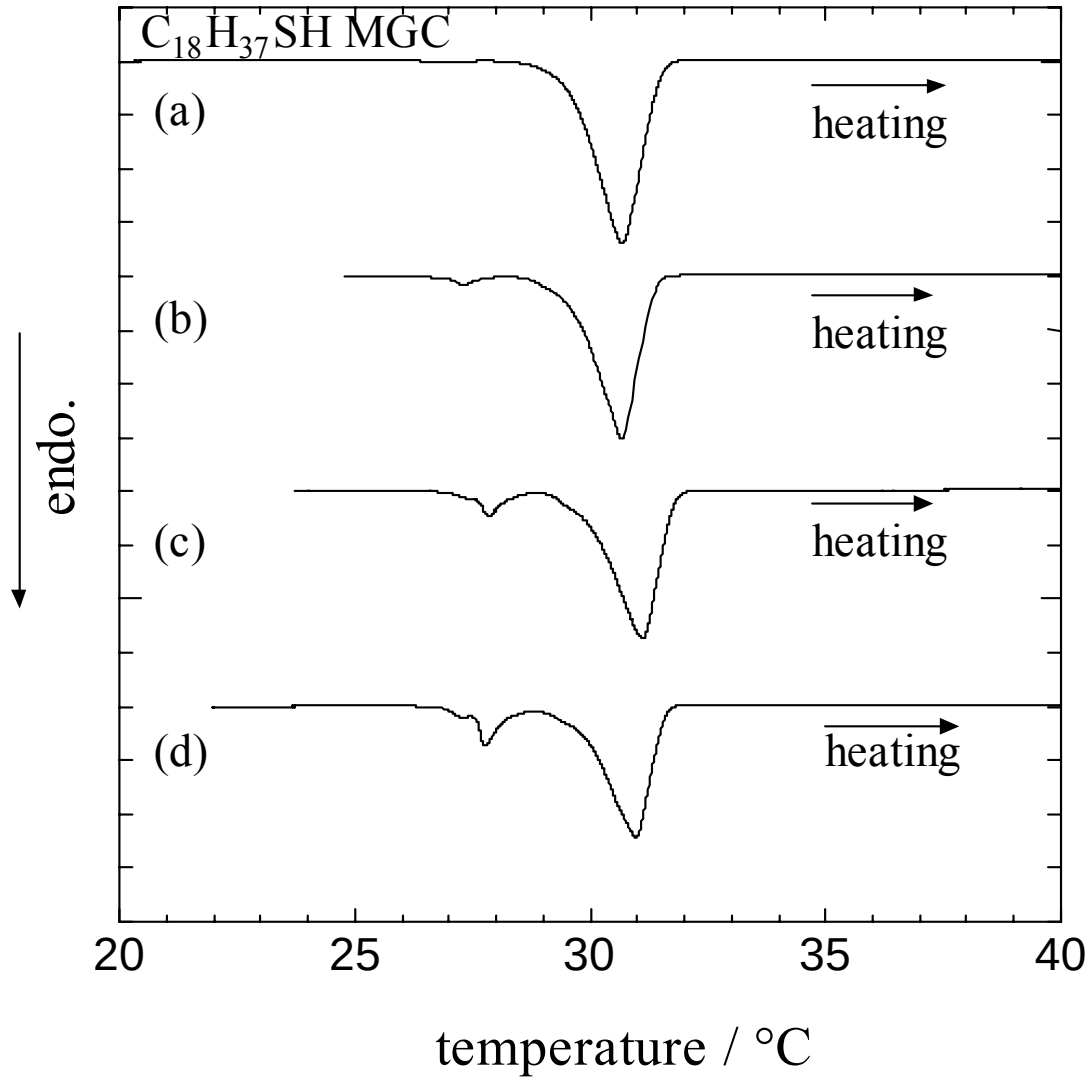

Figure 17 DSC heating thermograms of C18SH immediately after cooling from the melt to 20°C with cooling rate of, (a) 500°C/min, (b) 2°C/min (c) 1°C/min, and (d) 0.1°C/min.

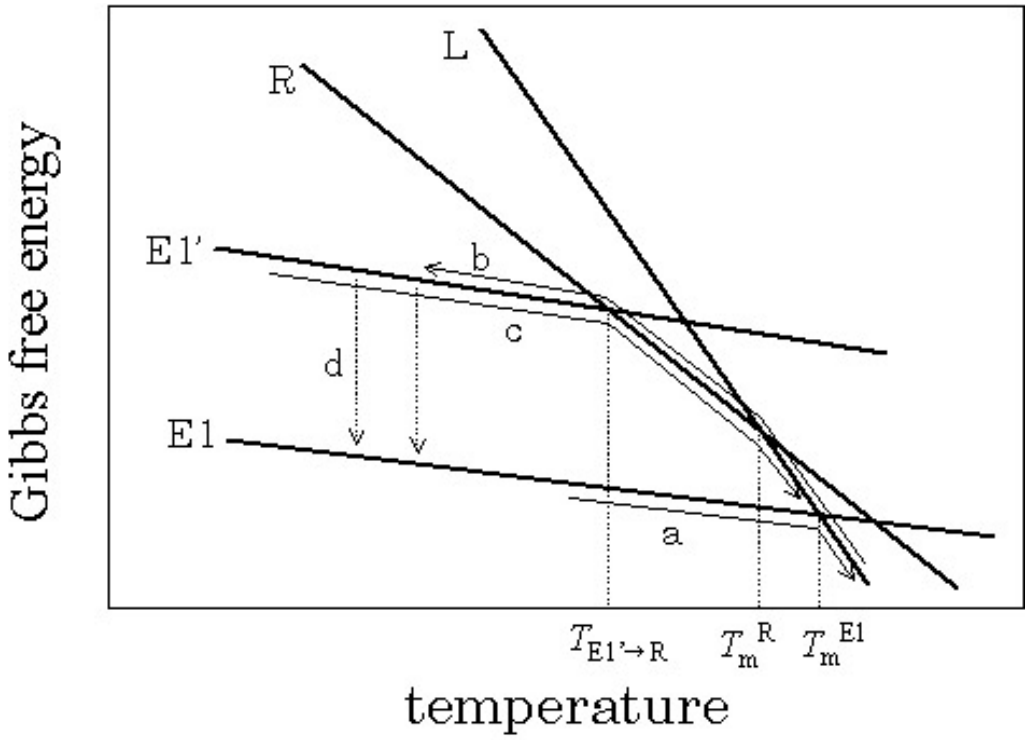

Figure 18 Relative free energy diagram of the alkanethiol with even carbon number. The temperatures, T_m^R and T_m^{E1}, are the melting points of the R phase and the E1 form, and $T_{E1'\rightarrow R}$ is the transition temperature of the E1'→R phase transition.

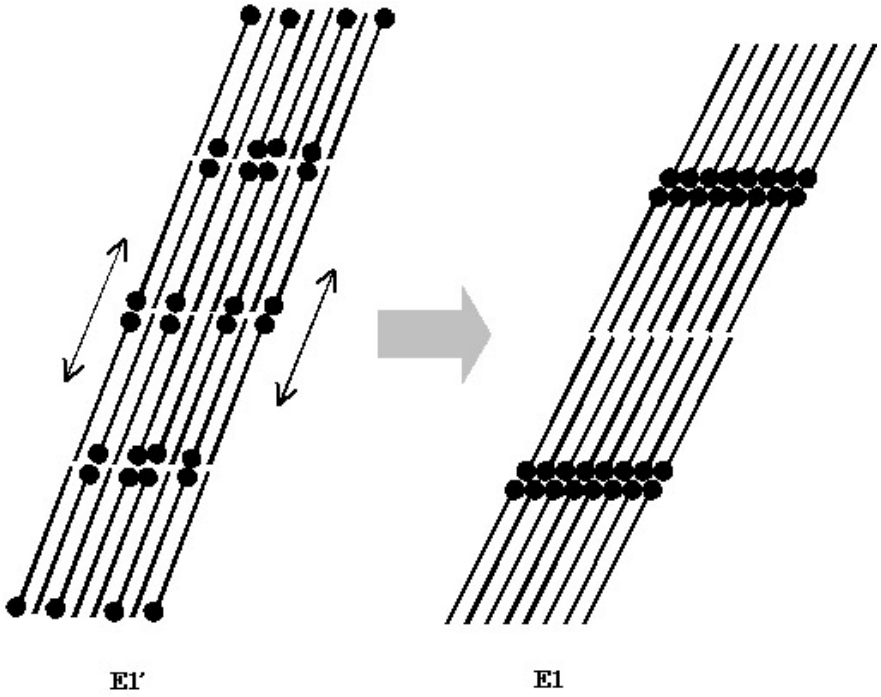

Figure 19 Schematic picture of the structural change model in the E1'→E1 phase transition. The dimer molecules in the E1' form translate along the chain axes, and the SH groups of the molecules may be arranged with the same side of the layer plane.

Table I Peak positions (2θ) and *d*-spacing of Bragg reflections in X-ray powder diffraction pattern of the E2 form of C19SH (SGC).

index	2θ (deg) for Cu-Kα radiation	*d*-spacing (nm)	intensity
0 0 1	1.81	4.88	strong
0 0 2	3.66	2.41	medium
0 0 3	5.49	1.61	medium
0 0 4	7.31	1.21	medium
0 0 5	9.14	0.968	weak
0 0 6	10.97	0.807	strong
0 0 8	14.65	0.605	strong
0 0 10	18.34	0.484	strong
1 1 0_s	21.97	0.405	very strong
2 0 0_s	23.96	0.371	strong

Table II Peak positions (2θ) and *d*-spacing of Bragg reflections in X-ray powder diffraction pattern of the E1 form of C22SH (SGC).

index	2θ (deg) for Cu-Kα radiation	*d*-spacing (nm)	intensity
0 0 2	3.21	2.75	very weak
0 0 3	4.74	1.86	very strong
0 0 4	6.32	1.40	medium
0 0 5	7.90	1.12	strong
0 0 6	9.48	0.933	medium
0 0 7	11.06	0.800	medium
0 0 8	12.65	0.700	medium
0 0 9	14.25	0.622	very weak
0 0 10	15.83	0.560	medium
0 0 12	19.03	0.466	medium
1 1 0_s	21.79	0.408	very strong
2 0 0_s	24.00	0.371	medium

Table III Peak positions (2θ) and *d*-spacing of Bragg reflections in X-ray powder diffraction pattern of the E1' form of C22SH (MGC).

index	2θ (deg) for Cu-Kα radiation	*d*-spacing (nm)	intensity
0 0 1	3.16	2.80	very weak
0 0 2	6.32	1.40	weak
0 0 3	9.50	0.931	weak
0 0 4	12.66	0.699	weak
0 0 5	15.84	0.560	weak
0 0 6	19.04	0.466	weak
1 1 0_s	21.70	0.410	very strong
2 0 0_s	23.84	0.373	strong

Table IV Phase transition temperature of *n*-alkanethiols determined by DSC.

alkanethiol	polymorph at room temperature	$T_{E1'\rightarrow R}$ (°C)	T_m^{R} (°C)	T_m^{E1} (°C)	T_m^{E2} (°C)
C18SH SGC	E1	-	-	30.2	-
C18SH MGC	E1'	27.0	27.5	-	-
C19SH SGC and MGC	E2	-	-	-	40.1
C22SH SGC	E1	-	-	46.0	-
C22SH MGC	E1'	41.1	44.6	-	-
C23SH SGC and MGC	E2	-	-	-	53.6
C24SH SGC	E1	-	-	51.9	-
C24SH MGC	E1'	45.1	51.2	-	-